THE JOURNAL OF BIOLOGICAL CHEMISTRY VOL. 287, NO. 48, pp. 40350–40359, November 23, 2012

Redox and Chemical Activities of the Hemes in the Sulfur Oxidation Pathway Enzyme SoxAX*[S]

Received for publication, June 28, 2012, and in revised form, September 26, 2012 Published, JBC Papers in Press, October 11, 2012, DOI 10.1074/jbc.M112.396192

Justin M. Bradley[‡], Sophie J. Marritt[‡], Margaret A. Kihlken[§], Kate Haynes[‡], Andrew M. Hemmings[‡], Ben C. Berks[§], Myles R. Cheesman[‡], and Julea N. Butt[‡1]

From the [‡]Centre for Molecular and Structural Biochemistry, School of Chemistry and School of Biological Sciences, University of East Anglia, Norwich Research Park, Norwich NR4 7TJ and the [§]Department of Biochemistry, University of Oxford, South Parks Road, Oxford OX1 3QU, United Kingdom

Background: SoxAX enzymes initiate microbial oxidation of reduced inorganic sulfur compounds. Their catalytic mechanism is unknown.
Results: Cyanide displaces the $CysS^-$ ligand to the active site heme following reduction by $S_2O_4^{2-}$ but not Eu(II).
Conclusion: An active site heme ligand becomes labile on exposure to substrate analogs.
Significance: Elucidation of SoxAX mechanism is necessary to understand a widespread pathway for sulfur compound oxidation.

SoxAX enzymes couple disulfide bond formation to the reduction of cytochrome *c* in the first step of the phylogenetically widespread Sox microbial sulfur oxidation pathway. *Rhodovulum sulfidophilum* SoxAX contains three hemes. An electrochemical cell compatible with magnetic circular dichroism at near infrared wavelengths has been developed to resolve redox and chemical properties of the SoxAX hemes. In combination with potentiometric titrations monitored by electronic absorbance and EPR, this method defines midpoint potentials (E_m) at pH 7.0 of approximately +210, −340, and −400 mV for the His/Met, His/Cys^-, and active site His/$CysS^-$-ligated heme, respectively. Exposing SoxAX to $S_2O_4^{2-}$, a substrate analog with E_m ~−450 mV, but not Eu(II) complexed with diethylene triamine pentaacetic acid (E_m ~−1140 mV), allows cyanide to displace the cysteine persulfide ($CysS^-$) ligand to the active site heme. This provides the first evidence for the dissociation of $CysS^-$ that has been proposed as a key event in SoxAX catalysis.

Microbial oxidation of reduced inorganic sulfur compounds forms an integral part of the biogeochemical sulfur cycle. It is exploited in biomining and is the defining metabolic pathway in both photosynthetic and nonphotosynthetic sulfur bacteria where it produces electrons that may be used for CO_2 fixation or fed into respiratory electron transfer chains (1, 2). The best studied and most widely distributed pathway for this process is the Sox[2] (sulfur oxidizing) pathway that converts thiosulfate and certain other sulfur species to sulfate (1). Intermediates in this pathway are covalently bound to a Cys residue in the SoxYZ protein. SoxYZ uses a swinging arm mechanism to deliver these intermediates to the active sites of the other Sox components (3, 4). SoxAX catalyzes the first step of the pathway in which thiosulfate is oxidatively coupled to the Cys of SoxYZ with the reduction of two molecules of cytochrome (cyt) *c*. SoxAX enzymes have been classified into three groups (5). Groups 1 and 2 are heterodimers containing three and two *c*-type hemes, respectively. Group 3 comprises diheme-containing heterotrimers with an additional SoxK subunit. Although details of the mechanism of thiosulfate and SoxY co-oxidation by SoxAX are unclear, it is likely that one of the roles of the hemes is to mediate electron transfer from substrates to cyt *c* (2).

The SoxAX enzymes of both *Rhodovulum sulfidophilum* and *Paracoccus pantotrophus* belong to group 1. In these enzymes, the SoxX subunit binds one heme with His/Met axial ligands, whereas both hemes in the larger SoxA subunit have the highly unusual His/thiolate axial ligand set (6–8). Crystal structures of both proteins reveal an almost linear constellation of hemes that have been labeled Heme-1, -2, and -3 in the convention of Bamford *et al.* (8). The heme of SoxX (Heme-3) and one heme of SoxA (Heme-2) are positioned close to the dimer interface such that their shortest edge-to-edge separation is of the order of 10 Å. By contrast, the second SoxA heme (Heme-1) is positioned ~24 Å from its neighbor, precluding physiologically relevant rates of intramolecular electron transfer to the other SoxAX hemes. In *Starkeya novella* SoxAX, the most studied of the diheme group 2 and 3 enzymes, the arrangement and ligation of the hemes straddling the dimer interface are conserved (9). In these enzymes, Heme-1 is replaced with a disulfide bond (10), and the role of either group in enzyme activity is unclear.

A solvent channel leads from the protein surface to the distal face of Heme-2, suggesting that this forms part of the active site for thiosulfate oxidation (6, 8, 9). Distal ligation of this heme is provided by a cysteine persulfide ($CysS^-$) formed by post-translational modification of Cys-222A (*R. sulfidophilum* numbering). This modification may arise from decomposition of a catalytic intermediate during enzyme purification. Alterna-

* This work was supported by grants from the Biotechnology and Biosciences Research Council (Grants B15211, C007808, B18695, G024758, and G009228) and the University of East Anglia.
[S] This article contains supplemental text, Figs. 1 and 2, and Tables 1 and 2.
The atomic coordinates and structure factors (code 2OZ1) have been deposited in the Protein Data Bank (http://wwpdb.org/).
[1] To whom correspondence should be addressed. Tel.: 44-1603-593877; Fax: 44-1603-592003. E-mail: j.butt@uea.ac.uk.
[2] The abbreviations used are: Sox, sulfur oxidizing; cyt *c*, cytochrome *c*; E_m, midpoint potential; MCD, magnetic circular dichroism; LMCT, ligand-to-metal charge transfer; nIR, near infrared; DTPA, diethylene triamine pentaacetic acid; $CysS^-$, cysteine persulfide; T, teslas; DMSO, dimethyl sulfoxide.

tively, conjugation of a sulfur atom to Cys-222A with the formation of $CysS^-$ could form a step in the pathway for thiosulfate oxidation in a mechanism similar to that of sulfur transferases such as rhodanese (11, 12). In such a mechanism, the oxidation of thiosulfate ($^-S\text{-}SO_3^-$) would not occur as an inner sphere reaction of the heme iron. Instead, dissociation of Cys^- from Heme-2 would facilitate the formation of a $Cys\text{-}SSO_3^-$ intermediate, and the heme would act simply as a conduit for electron transfer in the subsequent steps of the pathway. However, to date, there is no evidence for such an intermediate nor that the distal ligand $CysS^-$ can dissociate from the heme.

In contrast to the lack of chemical activity reported for the SoxAX hemes, these cofactors are known to be redox-active, and their midpoint potentials (E_m) are key to discussions of the mechanism of electron transfer from thiosulfate to cyt *c*. The His/Met-ligated Heme-3 has been assigned an E_m value of +190 mV for *P. pantotrophus* SoxAX and +162 mV for the *S. novella* enzyme, both values being consistent with those found for similarly ligated *c*-hemes in other proteins and compatible with electron transfer to cyt *c* (all potentials *versus* standard hydrogen electrode) (9, 13, 14). The His/thiolate-ligated heme(s) have much lower E_m values of approximately −430 and < −800 mV for *P. pantotrophus* SoxAX and −479 mV for *S. novella*. The *S. novella* enzyme has only one His/thiolate-ligated heme, and so Heme-2 must have $E_m = -479$ mV, whereas for *P. pantotrophus* SoxAX, an unambiguous assignment of E_m values to Heme-1 and -2 cannot be made. *R. sulfidophilum* SoxAX has been reported to have a His/thiolate-ligated heme resistant to reduction by dithionite ($E_m \sim -450$ mV) and thus with an E_m value lower than this chemical (7). However, Heme-2 and -3 have been proposed to act as a redox-linked pair with an E_m of +180 mV (8). Consequently, there is no unifying description of heme redox chemistry in the dimeric SoxAX enzymes, and this raises the possibility of variation in the mechanisms for thiosulfate oxidation within the SoxAX family. Alternatively, the assignment of E_m values in one or more of the proteins may be erroneous because the spectroscopic properties of the His/thiolate-ligated hemes make such measurements nontrivial.

Potentiometric titrations monitored by electronic absorption spectroscopy have typically been performed to define E_m values. However, reduction produces relatively little change in the electronic absorbance of a His/Cys^--ligated heme when compared with that displayed by its His/Met-ligated counterpart (15). This complicates the interpretation of potentiometric titrations of the tri-heme-containing SoxAX enzymes monitored by electronic absorbance because redox transitions of Heme-3 may mask those from either Heme-1 or Heme-2. However, this consideration is not relevant to interpreting potentiometry monitored by magnetic circular dichroism (MCD) where redox transitions of His/Met- and His/$Cys(S)^-$-ligated hemes can be distinguished with confidence. In the MCD of SoxAX, the His/$Cys(S)^-$-ligated hemes gives rise to a ligand-to-metal charge transfer band (LMCT) in the range 1050–1200 nm (9) when compared with 1800 nm for His/Met ligation (16). Potentiometric titration of *R. sulfidophilum* SoxAX monitored by nIR-MCD should then readily establish whether Heme-2 and -3 form a redox-linked pair with an E_m of ~+180 mV as suggested previously (8).

We report here an optically transparent electrochemical cell compatible with ambient temperature nIR-MCD. The cell has been employed to study redox transformations of *R. sulfidophilum* SoxAX driven by equilibration with the electrochemical potential applied to a gold electrode. The results have been complemented by those from other spectroscopies and parallel experiments investigating the products of reduction arising from equilibration of the enzyme with Eu(II) and dithionite. We are able to present a unified description of redox chemistry within the active site of SoxAX enzymes. We also demonstrate that dithionite, a potential substrate analog, is unique in inducing chemical reactivity at the active site heme. To our knowledge, this provides the first demonstration of such reactivity in this important class of enzymes.

EXPERIMENTAL PROCEDURES

Expression and Purification of Recombinant R. sulfidophilum SoxAX—A plasmid was constructed to allow heterologous expression of *R. sulfidophilum soxXA* in *Rhodobacter capsulatus* under the control of the dimethyl sulfoxide (DMSO)-inducible *dorA* promoter. *soxX* was amplified from *R. sulfidophilum* chromosomal DNA using primers MKS001 (5′-AGACTGGATCCATGCGAGGTATGG-3′) and MKS002 (5′-ACCGGACTAGTCATTGCGTCAGC-3′). The amplicon was digested with BamHI and ligated into BamHI- and SmaI-digested pGEM-7Zf(+) (Promega) to produce plasmid pMKSO1. *soxA*, together with the *soxA* ribosome binding site, were amplified from *R. sulfidophilum* chromosomal DNA using primers MKS003 (5′-ACTAGTCGTTGAGGCGCTCCGTCG-3′) and MKS006 (5′-TCTAGATCAGTTGCGGACCGACG-3′). The amplicon was digested with SpeI and XbaI and ligated into the same sites in pMKS01 to give plasmid pMKS08. The *soxXA* genes were excised from plasmid PMKS08 with BamHI and XbaI and cloned into the same sites in pDorex (17) to produce plasmid pMKS10. The *soxXA*-containing HindIII-XbaI fragment from pMKS10 was then cloned into the same sites in pRK415 (18) to give plasmid pMKS12.

Plasmid pMKS12 was introduced into *R. capsulatus* strain 37B4 Δ*dorA* (19) by conjugation from *Escherichia coli* strain S17-1 (20). Starter cultures were grown photoheterotrophically at 28 °C on malate-containing RCV medium (21) supplemented with 1 μg ml^{-1} tetracycline. 80 ml of starter culture at an $A_{600\,nm} \sim 3$ was used to inoculate 5-liter bottles of RCV-malate medium supplemented with 1 μg ml^{-1} tetracycline, 60 mM DMSO, and 1 mM sodium molybdate, and the resulting static cultures were incubated under illumination at 28 °C for 5 days. Cells were harvested, a periplasmic fraction was isolated, and the recombinant SoxAX protein was purified, all as described previously for SoxAX prepared from *R. sulfidophilum* (22) except that spheroplasts were prepared with buffer containing 1.5 mg ml^{-1} Na_2EDTA and 5 mg ml^{-1} lysozyme, and the perfusion chromatography polishing step was omitted. Purified SoxAX was quantified by electronic absorption spectroscopy using an extinction coefficient of 350 mM^{-1} cm^{-1} at 412.5 nm for the oxidized protein (7). Prior to spectroscopic analysis, samples of SoxAX were exchanged into buffer-electrolyte solu-

tions composed of reagents of AnalaR quality or equivalent and water of resistivity >18 megaohms cm.

Potentiometric Titration by Electrodic Equilibration—Optically transparent electrochemical cells of three designs were used to poise samples of SoxAX at various potentials for examination by (magneto-) optical spectroscopies. The cells employed three electrodes connected to an Autolab PGSTAT12 potentiostat under the control of the GPES software. The working electrode was selected to optimize the quality of data in terms of (*a*) spectral signal-to-noise and (*b*) the time needed for sample equilibration with the applied potential because this limited the number of potentials for which a spectrum could be collected over a practical time period.

Potentiometric titrations monitored by electronic absorbance were performed with a working electrode composed of mesoporous nanocrystalline SnO_2 in a previously described cell configuration (23, 24). SoxAX was adsorbed onto SnO_2 electrodes during 2 h of cyclic voltammetry (+60 mV to −540 mV, 20 mV s^{-1}) in 35 μM SoxAX, 50 mM Hepes, 100 mM NaCl, pH 7, 20 °C. The SoxAX loaded electrode was then rinsed with buffer-electrolyte to remove loosely bound material prior to placing it inside the spectroelectrochemical cell. Taking the extinction coefficient of adsorbed SoxAX to be the same as that of the protein in solution and the path length of the adsorbed sample to be the 4-μm thickness of the SnO_2 layer, a surface coverage of 1.2 nmol of SoxAX cm^{-2} geometric electrode area was calculated. These electrodes typically have a surface area 300× the geometric area (25). Thus, SoxAX coverage corresponded to 4 pmol cm^{-2}, which for a protein with dimensions of ~34 × 36 × 75 Å indicates good penetration of protein into the mesoporous structure.

Spectropotentiometric titrations monitored by MCD in the visible region were performed in an optically transparent electrochemical cell (1-mm path length) with a working electrode composed of a gold mini-grid as described previously (26). The samples typically contained 53 μM SoxAX in 50 mM Hepes, 100 mM NaCl, pH 7, and 40 μM each of the following mediators: methylene blue, 2,6-dichlorophenolindophenol, phenazine methosulfate, ferricyanide, diaminodurene, anthraquinone-2,6-sulfate, anthraquinone-2-sulfate, benzyl viologen, and methyl viologen.

At near infrared (nIR) wavelengths, it was found that gold mini-grid electrodes were depolarizing and that the SnO_2 electrodes were not transparent when they were conducting. As a consequence, potentiometric titrations of mediated SoxAX solutions monitored by MCD at nIR wavelengths were performed with a modification of the cell used for MCD at visible wavelengths. The mini-grid working electrode was replaced by a ribbon of gold foil folded to an "S"-shape 2 mm wide and 4 mm high. The gold ribbon was 1 mm wide so that when the "S" was inserted into the cell, the working faces of the electrode spanned the path length of the cell. The front window of the cell was masked off to ensure that only the sample within ~0.5 mm of the extremities of the working electrode lay in the light path. In this way, equilibration with applied potential, that is, reliant on diffusion of protein and redox mediators to the electrode, could be achieved within ~30 min. Spectra collected during MCD-monitored potentiometry in both the UV-visible and the nIR regions are presented without base-line correction.

Preparation of Chemically Poised Samples for MCD and EPR Spectroscopy—Samples of SoxAX (200 μM) in 50 mM Hepes, 100 mM NaCl, D_2O, pH* 7 (where pH* is the apparent pH of the D_2O solution determined using a standard glass pH electrode) were chemically poised at defined potentials in a sealed vessel housed in a nitrogen-filled chamber as described previously (27). Aliquots of chemical reductants/oxidants were titrated into the sample until equilibration at the desired potential was achieved and during which time the sample was stirred and maintained at 4 °C. Equilibrated samples were rapidly transferred to an anaerobic MCD cell for analysis by room temperature nIR-MCD or into EPR tubes and frozen. Samples of fully oxidized SoxAX were prepared by the addition of potassium ferricyanide, whereas samples poised at +45, −360, and −500 mV were prepared by reduction with ascorbate, Eu(II), and Eu(II) complexed by diethylene triamine pentaacetic acid (DTPA), respectively (28). To facilitate equilibration at a measurable potential, each experiment included 40 μM of each of the following mediators: trimethylhydroquinone, menadione, 5-hydroxynaphthoquinone, and methylene blue. For poising at −360 and −500 mV, the samples additionally contained 40 μM each of benzyl viologen, sulfonyl viologen, and methyl viologen. Stock solutions of $EuCl_2$ (20 mM) were prepared anaerobically and immediately prior to use by dissolution of the desired mass in 50 mM Hepes, 100 mM NaCl, D_2O, pH* 7. A stock solution of DTPA was prepared in 0.2 M NaOH, D_2O.

Preparation of Samples with Cyanide-ligated Heme—Samples for optical spectroscopy comprised either 40 μM (electronic absorbance) or 100 μM (nIR-MCD) SoxAX in 50 mM Tris/HCl, pH 7.8, or 50 mM Tris/HCl, pH* 7.8 D_2O, respectively. Reduction of the samples was carried out in a nitrogen-filled chamber by the addition of sequential aliquots of either a 5 mM solution of sodium dithionite or a saturated (25 mM) solution of Eu(II)DTPA prepared as described above. Aliquots of KCN were titrated into the samples to produce the maximum change in the electronic absorbance spectra. Samples for EPR spectroscopy were prepared in a similar fashion with a protein concentration of 114 μM. The sample was transferred to an EPR tube and frozen prior to measurement. Between measurements, the sample was thawed, in a nitrogen-filled chamber if necessary, to allow the addition of dithionite or KCN or air equilibration, the consequences of the chemical manipulations being monitored using electronic absorbance spectroscopy.

Spectroscopy—Electronic absorption spectra were recorded on either a Hitachi U4100 or a Hitachi U2900 spectrophotometer. MCD spectra were recorded using circular dichrographs, JASCO models J810 and J730 for the UV-visible and nIR regions, respectively. Either an Oxford Instruments SM1 split-coil superconducting solenoid with a 25-mm ambient temperature bore or an Oxford Instruments Special Spectromag 1000, a bespoke split-coil superconducting solenoid with a 50-mm ambient temperature bore, was used to generate a magnetic field of 6 T for the ambient temperature MCD measurements. EPR spectra were recorded on a spectrometer comprising an ER-200D electromagnet and microwave bridge interfaced to an EMX control system (Bruker, Spectrospin) and fitted with a

liquid helium flow cryostat (ESR-9, Oxford Instruments) and a dual mode X-band cavity (Bruker, type ER4116DM). EPR spectra were simulated using the Bruker WinEPR and SimFonia software and quantified by double integration of the simulated component spectra.

Global Analysis of Potentiometric Data—Ambient temperature methods allow the convenience of measuring the spectrum of a single sample across a wide range of electrochemical potential applied *in situ*. However, none of the spectroscopic techniques suitable for monitoring ambient temperature potentiometry were capable of resolving the different responses of the two thiolate-ligated hemes of SoxAX as was possible through the EPR of frozen samples. As a consequence, the midpoint potentials of the three SoxAX hemes were obtained from a global analysis of the potentiometric data collected from all of these approaches. Six data sets were included in this analysis. Five of these arose from optically monitored potentiometry: variation of signal intensity with potential from i) electronic absorbance at 552–565 nm (25 data points), ii) MCD at 548–553 (10 data points), iii) MCD at 1170 nm (20 data points), iv) MCD at 1800 nm (11 data points), and v) MCD at 1500 nm (11 data points). The sixth data set quantified the EPR intensity attributed to the LS1 and LS2 species as a function of potential (4 data points).

For each data set, the variation in intensity with potential was assumed to arise from the sum of the intensities arising from three hemes acting as independent sites undergoing single electron oxidation/reduction in a manner described by the Nernst equation

$$y_{\mathrm{calc}(i)} = \sum_n A_n/\{1 + F/RT^{\exp}(x_{(i)} - E_{m(n)})\} \qquad \text{(Eq. 1)}$$

where $y_{\mathrm{calc}(i)}$ is the calculated normalized intensity of point i, A_n is the fractional intensity attributed to heme n, F is the Faraday constant, R is the ideal gas constant, T is the temperature, $x_{(i)}$ is the potential of point i, and $E_{m(n)}$ is the midpoint potential of heme n. The midpoint potential of each heme was constrained to be identical for each data set examined. The fractional change in intensity contributed by each heme to each data set was parameterized in the model but held constant during refinement when the value could be determined *a priori* by consideration of the system. The latter was the case for (*a*) the nIR-MCD intensity at 1500 and 1800 nm that must arise solely from the His/Met-ligated heme and (*b*) the EPR intensity that must have equal contribution (33.3%) from each heme for fully oxidized SoxAX. Thus, six data sets were simultaneously analyzed using 81 data points to define 12 refined parameters, namely, three E_m values and nine fractional contributions to signal intensity.

The algorithm simultaneously analyzed the 81 data points using the Levenberg-Marquardt method to minimize the function

$$\chi^2 = \left(\sum_i \frac{(y_{\mathrm{calc}}(i) - y_{\mathrm{obs}}(i))^2}{\sigma(i)^2} \right) \Big/ i \qquad \text{(Eq. 2)}$$

where $y_{obs}(i)$ is the intensity of the ith data point and $\sigma(i)$ is the estimated standard deviation of $y_{obs}(i)$. $y_{calc(i)}$ is defined above. The best fit to the experimental data was obtained using the parameters described in Table 3, yielding a χ^2 of 7. The major features of all data sets are well described by this model, the main difference between calculated and observed behavior being due to residual intensity in the 1500 nm MCD response between 0 and +100 mV. Accounting for this feature in a model assuming Nernstian behavior would require the introduction of a fourth oxidation/reduction event not evident in any of the other data sets. Constraining the fractional intensities at the selected wavelengths at ~550 nm in the electronic absorbance and MCD data to be equal for both low potential hemes led to a 60% increase in χ^2. Constraining the heme with the lowest E_m to give the lowest amplitude responses in these data sets led to a doubling of χ^2. The significantly lower quality of the fits in these cases, indicated by the higher χ^2 values, was caused by the model predicting that 550 nm absorbance increased at more positive potentials than observed.

RESULTS

Overview of the Properties of Recombinant SoxAX—A system for the heterologous expression of *R. sulfidophilum* SoxAX in *R. capsulatus* was developed to provide sufficient SoxAX protein for detailed spectroelectrochemical analysis. The recombinant *R. sulfidophilum* SoxAX protein crystallized in space group $P2_1$. The asymmetric unit had dimensions similar to those found in the 2.55 Å structure of the native protein (8) and contained four copies of SoxAX. The structure of the recombinant protein is essentially identical to that of the native protein (supplemental Fig. 1) with an overall average root mean square deviation of 0.26 Å (supplemental Table 1). Ligation of all three SoxAX hemes was the same as in the native structure. All four monomers of the asymmetric unit had $CysS^-$ ligation of the active site Heme-2, although the recombinant SoxAX protein had been produced in the absence of thiosulfate or other Sox pathway components (supplemental Fig. 2). Equivalent turnover-independent modification of the active site heme ligand has also been reported for another recombinant SoxAX protein (9).

The nIR-MCD spectrum of fully oxidized recombinant protein at ambient temperature (Fig. 1) was indistinguishable from that of the wild-type enzyme (7). Prominent features were present at 1170 and 1800 nm that have been assigned to the LMCT bands from the $His/Cys(S)^-$ (29, 30)- and His/Met (16)-ligated ferric hemes, respectively. A broader feature of lower intensity spans the range 1300–1600 nm and arises from the vibrational sidebands of the peak at 1800 nm. The spectral features of the oxidized recombinant protein when viewed by X-band EPR (Fig. 2) and MCD in the UV-visible region (Fig. 3*A*) were also indistinguishable from those of wild-type enzyme (7). The recombinant enzyme, henceforth simply referred to as SoxAX, was used in all studies presented below.

Potentiometric Titrations—In contrast to the prominent nIR-MCD arising from low-spin ferric hemes (Fig. 1), the corresponding LMCT transitions of their ferrous counterparts are symmetry-forbidden (31). Consequently, potentiometric titration monitored by nIR-MCD affords the opportunity to resolve the redox properties of hemes closely matched in midpoint potential but differing in axial ligation, as postulated for *R. sul-*

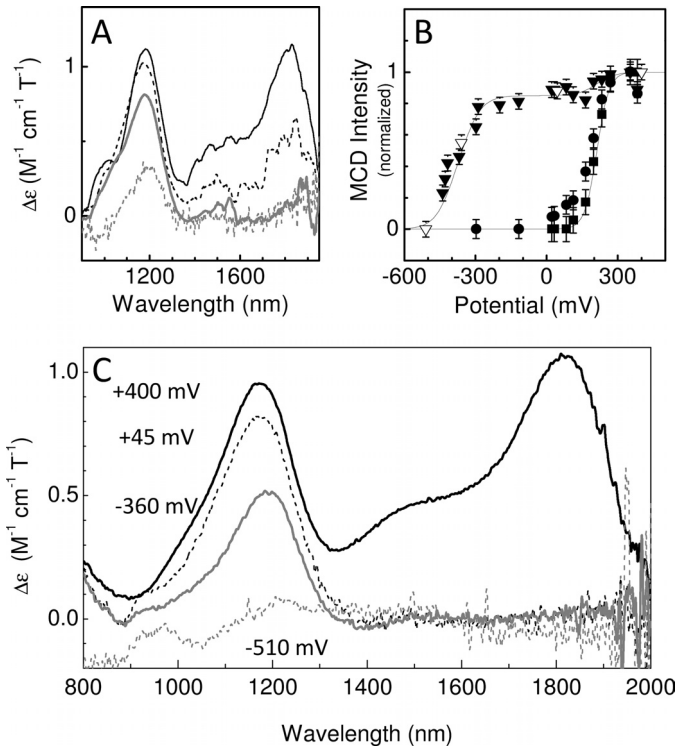

FIGURE 1. **Potentiometric titration of SoxAX monitored by nIR-MCD spectroscopy.** *A*, spectra of 160 μM SoxAX electrodically poised at increasingly negative potentials of +350 (*solid black*), +200 (*broken black*), −300 (*solid gray*), and -440 (*broken gray*) mV. *B*, normalized MCD signal intensity at 1800 (■), 1500 (●), and 1170 nm (▼) as a function of equilibration potential; data were collected for oxidative and reductive titrations. *Solid lines* indicate the intensity predicted for Nernstian behavior of three independent $n = 1$ centers described by the parameters listed in Table 3. *Open data points* represent chemically poised samples. *C*, spectra of 200 μM SoxAX chemically poised at +400, +45, −360, and −510 mV using air, ascorbate, Eu(II), and Eu(II)DTPA, respectively. The greater noise in the spectra of *A* when compared with *C* reflects the smaller area of the sample interrogated spectroscopically in the electrochemical cell when compared with a standard cuvette. Experiments were performed in 50 mM Hepes, 100 mM NaCl, D_2O buffer with pH* = 7.0.

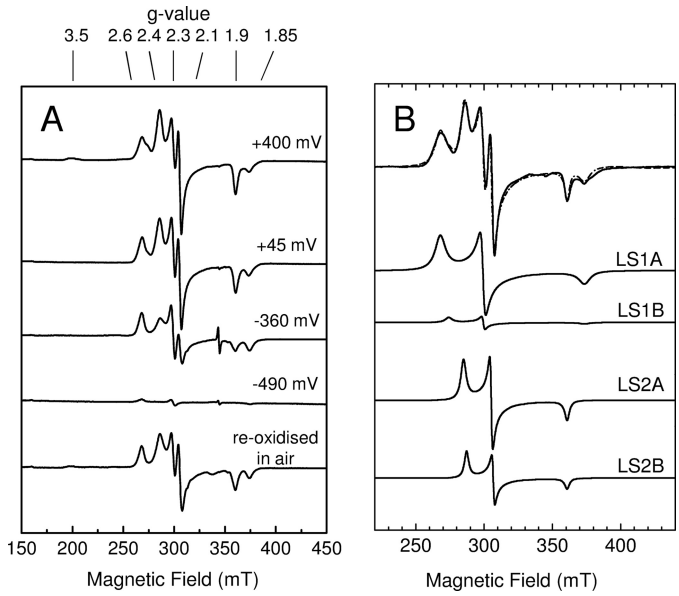

FIGURE 2. **Perpendicular mode X-band EPR spectra of SoxAX.** *A*, spectra of SoxAX chemically poised at +400, +45, −360, and −490 mV with air, ascorbate Eu(II), and Eu(II)DTPA, respectively, and for the sample poised at −490 mV following reoxidation in air. Sample conditions are as in Fig. 1. Spectrometer parameters: microwave frequency 9.68 GHz, microwave power 2 milliwatts, modulation amplitude 10 G, and temperature 20 K. *B*, the spectrum of SoxAX poised at +400 mV together with its simulation by contributions from LS1a, LS1b, LS2a, and LS2b with the parameters and proportions indicated in Tables 1 and 2. The sum of the simulated contributions is indicated by the *broken line* in the *upper trace*.

fidophilum SoxAX (8), because the energy of the LMCT for the ferric hemes will differ. To exploit this possibility, a thin layer electrochemical cell optically transparent to circularly polarized light of nIR wavelengths was developed as described under "Experimental Procedures." The effect of electrochemical potential on the nIR-MCD of SoxAX is summarized in Fig. 1, *A* and *B*. When poised at potentials above +300 mV, SoxAX yields spectra that are typical of the fully oxidized enzyme. Lowering the sample potential to 0 mV removed all MCD intensity at wavelengths above 1400 nm and produced a small (15%) drop in the intensity of the feature at 1170 nm. Between 0 and −300 mV, the spectra were indistinguishable. Equilibrating at lower potentials produced a decrease in the intensity of the 1170 nm feature such that at −440 mV, it had 20% of that displayed by fully oxidized enzyme. Poising the sample at increasingly positive potentials reversed the spectral changes seen on reduction and demonstrated the reversibility of the events being monitored.

Attempts to equilibrate samples below −440 mV and generate fully reduced SoxAX, as evidenced by the absence of intensity in the nIR-MCD, were unsuccessful as current continued to flow from the samples even after the desired potential had been applied for several hours. Consequently, SoxAX was chemically poised at four potentials selected to confirm and extend the description of its redox chemistry (Fig. 1*C*). The spectrum of SoxAX poised at +400 mV was again characteristic of the fully oxidized enzyme. Poising the sample at +45 mV was sufficient to remove all intensity at wavelengths above 1400 nm, and the sample poised at −360 mV showed a 40% reduction in the intensity at 1170 nm when compared with the fully oxidized sample in line with the results from the nIR-MCD compatible electrochemical cell (Fig. 1*B*). Significantly, poising SoxAX at −510 mV was sufficient to remove all MCD intensity above 800 nm, demonstrating complete reduction of the hemes. Taken together with the potentiometric data monitored by nIR-MCD, this demonstrates that the redox activity of the low-spin hemes is confined to two windows of potential, namely, +300 to 0 mV and −300 to −500 mV.

The peaks in the MCD at 1800 and 1170 nm arise from the LMCT transitions of His/Met- and His/Cys(S)$^-$-ligated ferric heme, respectively (16, 29, 30). Consequently, the His/Met-ligated Heme-3 is seen to undergo redox transformation between +300 and 0 mV, Fig. 1*B*. At least one of the His/thiolate-ligated hemes must undergo redox transformation between −300 and −500 mV. However, nIR-MCD does not allow unambiguous assignment of redox transformation of the second His/thiolate-ligated heme to either window of potential because there are various possible origins for the change in intensity of the 1170 nm feature between +300 and 0 mV. The intensity of heme LMCT transitions is determined in part by axial ligand orientation and so may vary widely for the same ligand set (16). This precludes the confident assignment of

$\Delta\epsilon_{1170\ nm}$ values to Heme-1 and -2 by comparison with the nIR-MCD response of other hemoproteins having His/Cys^- ligation or that of the His/$CysS^-$-ligated Heme-2 of the *S. novella* enzyme, respectively. The loss in 1170 nm intensity may reflect redox transformation of one of the SoxA hemes or simply a change in ligand orientation at one or both of these hemes in response to the reduction of Heme-3. Alternatively, the spectroscopic response of Heme-1 and -2 may be invariant at potentials greater than −300 mV with the change in 1170 nm intensity at high potential reflecting the loss of the "tail" of the feature at 1800 nm.

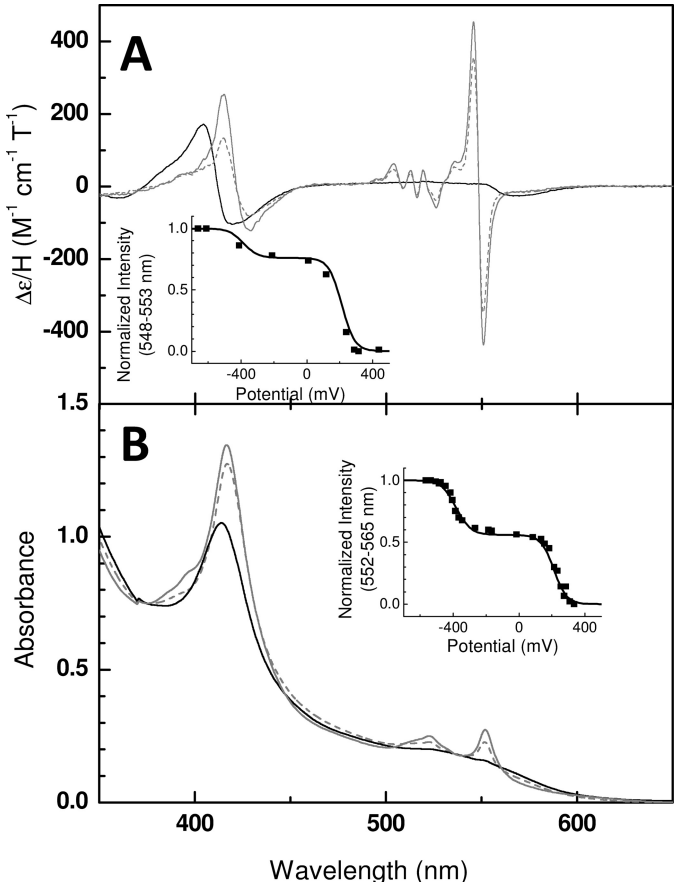

FIGURE 3. **Potentiometric titration of *R. sulfidophilum* SoxAX monitored by electronic absorbance and MCD spectroscopy in the visible region.** *A*, room temperature MCD spectra of 53 μM SoxAX poised at +450 (*black*), −200 (*broken gray*), and −500 mV (*solid gray*) by equilibration with a gold mini-grid electrode. *Inset* shows the intensity at 548 nm minus 553 nm as a function of equilibration potential. *B*, electronic absorbance spectra of SoxAX adsorbed on a nanocrystalline mesoporous SnO_2 electrode poised at +230 (*black*), −270 (*broken gray*), and −540 mV (*solid gray*). The features arising from SoxAX are superimposed on the scattering background arising from the nanocrystalline mesoporous SnO_2 electrode. *Inset* shows the intensity at 552 nm minus that at the 565 nm isosbestic point as a function of potential. *Solid lines* in both insets indicate the intensity predicted for Nernstian behavior of three independent $n = 1$ centers described by the parameters listed in Table 3.

For independent assessment of the redox properties of the His/$Cys(S)^-$-ligated Heme-1 and -2, they were probed further by the EPR of frozen SoxAX solutions chemically poised at potentials guided by the optical data collected at ambient temperatures (Fig. 2*A*). The X-band EPR of oxidized SoxAX is dominated by multiple rhombic trios between 260 and 380 mT characteristic of His/thiolate-ligated ferric hemes, whereas Heme-3 gives rise to a much smaller feature at $g_z = 3.48$. Each of these hemes is EPR-silent in the ferrous state. Poising of samples at +45 mV removes the feature at $g = 3.48$, consistent with reduction of the His/Met-ligated Heme-3 (Fig. 2*A*). The sample poised at −490 mV was essentially EPR-silent, indicating reduction of all three SoxAX hemes.

Quantification of the effect of intermediate potentials on the EPR of SoxAX required spectral simulation. Although Heme-3 gives rise to only one detectable feature, the resonances from Heme-1 and -2 can only be satisfactorily simulated using four rhombic components (Fig. 2*B*). The latter are grouped into two sets (Table 1). As described previously (7), these are termed LS1 and LS2, each of which is composed of two components, a and b, reflecting minor heterogeneities. The total EPR intensity arising from ferric Heme-1 and -2 in the sample poised at +45 mV is within error of that from fully oxidized SoxAX (Table 2). Thus, neither of these hemes is redox-active between +300 and 0 mV. The redistribution of the LS1 and LS2 intensity between the four contributing species in these samples is indicative of changes in ligand orientation at Heme-1 and/or Heme-2 in response to reduction of Heme-3. This accounts, at least in part, for the change in MCD intensity at 1170 nm across this potential range. Significantly, the sample poised at −360 mV displayed 50% of the LS2 intensity and 100% of the LS1 intensity displayed by fully oxidized SoxAX (Table 2). Therefore, the species giving rise to LS1 EPR signals must have a lower E_m value than those giving rise to the LS2 features.

Determining the two E_m values describing redox transformation of the thiolate-ligated hemes requires spectral resolution with high-fidelity across the potential domain. Consequently, two further ambient temperature spectroscopies allowing for precisely defined and *in situ* potentiometric control were employed, namely MCD and electronic absorption in the visible region. MCD in the wavelength range 300–700 nm contains features from both ferric and ferrous hemes that additionally inform on their spin state (32). Spectra recorded for potentials ranging from +450 to −500 mV showed no indication of positive intensity at ~430 nm or negative intensity at ~630 nm that would indicate high-spin ferrous and ferric heme, respectively (Fig. 3*A*). Instead, the spectral changes were characteristic of the interconversion of low-spin ferric and low-spin ferrous heme. These effects were quantified using the potential dependence of the peak-to-trough intensity at ~550 nm arising

TABLE 1
Parameters describing the rhombic features in EPR spectra of as purified SoxAX

	g_z	g_y	g_x	W_z	W_y	W_x
				mT	*mT*	*mT*
LS1a	2.578	2.312	1.851	3.6	1.5	4.5
LS1b	2.524	2.310	1.851	3.5	1.5	4.5
LS2a	2.409	2.255	1.917	2.2	1.3	2.3
LS2b	2.428	2.266	1.917	2.7	1.3	2.3

from low-spin ferrous heme (Fig. 3*A*, *inset*). More rapid equilibration of SoxAX across a wide potential window and thus greater spectral resolution across the electrochemical potential domain was achieved through its adsorption on an optically transparent SnO_2 electrode. Equilibration with the applied electrode potential was almost instantaneous as monitored by electronic absorption in the visible region such that the reversibility of SoxAX redox chemistry could be assessed over multiple cycles (Fig. 3*B*). Interconversion of features typical of low-spin ferric ($\epsilon_{412\ nm}$ 350 $mM^{-1}\ cm^{-1}$, $\epsilon_{553\ nm}$ 45 $mM^{-1}\ cm^{-1}$) and low-spin ferrous enzyme ($\epsilon_{420\ nm}$ 550 $mM^{-1}\ cm^{-1}$, $\epsilon_{555\ nm}$ 100 $mM^{-1}\ cm^{-1}$) was observed and quantified by the variation in the difference between the absorbance at 552 nm and that of the isosbestic point at 565 nm with potential (Fig. 3*B*, *inset*).

The optically monitored titrations confirmed that the redox chemistry of SoxAX is confined to the interconversion of low-spin ferric/ferrous heme and the two windows of potential identified by nIR-MCD-monitored potentiometry. As a consequence, a global analysis was employed to produce a model describing all of the potentiometric data through the sum of three independent Nernstian responses for single electron centers as described under "Experimental Procedures." All data sets, *i.e.* the plots of intensity *versus* potential, were modeled satisfactorily using the same set of E_m values: +210 mV for the His/Met-ligated Heme-3 and −340 and −400 mV for the thiolate-ligated hemes (Table 3 and *solid traces* in Fig. 1*B* and the *insets* of Fig. 3). This validates the results obtained using the novel nIR-MCD compatible electrochemical cell.

Although both thiolate hemes are found to contribute equally to the intensity change monitored by nIR-MCD, it is striking that the intensity change monitored by both electronic absorption and MCD spectroscopies in the visible region is dominated by the thiolate-ligated heme with the lower midpoint potential. The change in intensity observed at ~550 nm is typically much larger when thiolate-ligated ferric heme is reduced to ferrous thiol-, rather than thiolate-, ligated heme (33–35) because the absorbance band of the porphyrin π-π^* transition is much sharper in the former case. The intensity of the sharp features in this region of both the MCD and the electronic absorbance spectra of SoxAX clearly increases at low potential, with the best fit to the data being obtained when these changes are attributed to the heme with the lowest midpoint potential. Thus, we propose that the thiolate ligand to the heme of SoxAX with E_m −400 mV is protonated on reduction, whereas that to heme with E_m −340 mV is not. *S. novella* SoxAX, in which Heme-1 is absent, displays similar spectral changes at low potential, and in this light, we assign *R. sulfidophilum* Heme-2 an E_m value of −400 mV and attribute the LS1 EPR to this center.

Ligand Binding to SoxAX—The reactivity of SoxAX toward the potential exogenous ligand CN^- was screened using electronic absorbance spectroscopy (Fig. 4*A*). Enzyme incubated with excess CN^- in aerobic buffer had a spectrum similar to that of the enzyme as purified. The same was true for a sample reduced anaerobically with Eu(II)DTPA, equilibrated with excess CN^-, and then re-equilibrated with air. EPR spectroscopy confirmed the small changes to the absorbance spectrum to arise from displacement of the methionine ligand of Heme-3 by CN^- (not shown). By contrast, when the latter experiment was repeated using dithionite as the reductant, there was a 10% increase in the absorbance at 413 nm when compared with that of the other samples. The increase in electronic absorbance suggested that exposure to dithionite and cyanide produces a change of SoxAX heme ligation distinct to that produced by exposure to cyanide alone. This was confirmed and quantified by EPR and MCD spectroscopy (Fig. 4, *B* and *C*). Loss of the rhombic EPR features associated with LS1 species indicates displacement of thiolate as a ligand to Heme-2. As a consequence, the 50% reduction in 1170 nm MCD intensity shows Heme-2 to have $\Delta\epsilon$ of ~0.5 $M^{-1}\ cm^{-1}\ T^{-1}$, which compares favorably with the value of 0.46 $M^{-1}\ cm^{-1}\ T^{-1}$ predicted from global analysis of the potentiometric data (Table 3). The loss of MCD intensity at 1170 nm is accompanied by loss of all intensity at 1800 nm, the emergence of a new LMCT peak at 1650 nm, and increased EPR intensity at g ~3.4. Together these data indicate that after reaction of the enzyme with dithionite and CN^-, Heme-2 in addition to Heme-3 has His/CN^- ligation (16), whereas Heme-1 retains His/thiolate ligation.

Our attempts to use x-ray crystallography to resolve the structure of CN^--bound SoxAX were unsuccessful. We failed to find conditions where CN^--bound SoxAX would crystallize. We also failed to resolve any changes in the structure of SoxAX when crystals of the as prepared enzyme were soaked with dithionite and cyanide. Both results are consistent with SoxAX

TABLE 2
Relative contributions of the rhombic features to EPR spectra of SoxAX

	Total spin integration[a]	% of one heme equivalent[b]			
		LS1a	LS1b	LS2a	LS2b
	%				
Sample					
+400 mV	100	82	22	29	67
+45 mV	108	97	9	28	66
−360 mV	73	100	0	15	30
−490 mV	0	0	0	0	0

[a] Relative intensity of the thiolate envelope to that at +400 mV.
[b] Taking the sum of the spin integrations of the rhombic features at +400 mV to be equivalent to two hemes.

TABLE 3
Predicted midpoint potentials and optical properties of the hemes of SoxAX

E_m	$\epsilon_{552} - \epsilon_{565}$[a]	$\Delta\epsilon_{548} - \Delta\epsilon_{553}$[b]	$\Delta\epsilon_{1170}$[c]	$\Delta\epsilon_{1800}$[c]	Ligand assignment[d]
	$M^{-1}\ cm^{-1}$	$M^{-1}\ cm^{-1}\ T^{-1}$	$M^{-1}\ cm^{-1}\ T^{-1}$	$M^{-1}\ cm^{-1}\ T^{-1}$	
+210 mV	31,000	680	0.14	1.0	His/Met
−340 mV	3,400	70	0.40	0.0	His/thiolate
−400 mV	22,000	150	0.46	0.0	His/thiol

[a] Difference between the electronic absorbance at 552 nm and the 553 nm isosbestic point.
[b] Peak-to-trough intensity of the ferrous form in the visible region MCD.
[c] nIR-MCD intensity of the ferric form.
[d] Ligand assignment of the ferrous from.

undergoing conformational change on dissociation of the heme ligands, and further experiments are underway to identify the nature of these changes. As a consequence, further insight into the reactivity of SoxAX was obtained from spectroscopic studies. SoxAX reduced anaerobically with dithionite, reoxidized by equilibration with air, and then exposed to cyanide displayed spectroscopic changes identical to those when cyanide was introduced prior to reoxidation of the enzyme (not shown). In contrast, very little change is observed in the EPR of SoxAX that has been reduced with dithionite and reoxidized by equilibration with air but *not* exposed to CN^- (Fig. 4*B*), indicating thiolate ligation of both Heme-1 and Heme-2 in this case. The ability of Heme-2 to bind CN^- is therefore induced by dithionite, or one of its oxidation products, rather than simply by reduction of that heme. This reactivity persists when the enzyme is returned to the all-ferric state despite the retention of thiolate as a ligand to Heme-2 in the absence of CN^-.

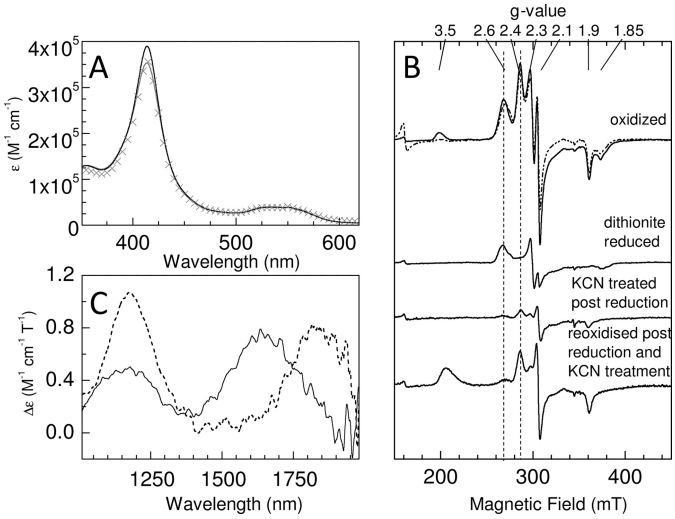

FIGURE 4. **Binding of CN^- to redox-cycled SoxAX.** *A*, electronic absorbance spectra of ferric SoxAX exposed to a 250-fold excess of KCN (*gray*) and reduction with dithionite (*black*) or Eu(II)DTPA (*gray crosses*) followed by exposure to a 250-fold excess of KCN and equilibration with air. *B*, X-band EPR of 114 μM SoxAX in the ferric state as purified, following reduction with sodium dithionite, following reduction with sodium dithionite and exposure to a 250-fold excess of KCN, and following reduction with sodium dithionite, exposure to a 250-fold excess of KCN, and reoxidation in air. The *broken trace* shows the spectrum of enzyme that has been reduced with sodium dithionite and reoxidized in air but not exposed to KCN. Spectrometer parameters: microwave frequency 9.68 GHz, microwave power 2 milliwatts, modulation amplitude 10 G, and temperature 20 K. *C*, nIR-MCD of SoxAX as purified (*broken black*) and following reduction with sodium dithionite, exposure to a 250-fold excess of KCN, and reoxidation in air (*solid black*). The lower intensity of the feature at 1800 nm relative to that at 1170 nm when compared with Fig. 1 is consistent with the partial reduction of Heme-3 in the enzyme as purified.

DISCUSSION

We find no evidence to support the previous report that Heme-2 and -3 form a redox-linked pair in *R. sulfidophilum* SoxAX (8). Instead, the active site His/$CysS^-$-ligated Heme-2 has an E_m that is some 600 mV lower than that of the His/Met-ligated Heme-3 (+210 mV). The E_m values are consistent with those reported for the hemes located at the interface between SoxA and SoxX in the tri-heme *P. pantotrophus* and diheme *S. novella* enzymes. Similar behavior is also likely for the group 3 SoxAX of *Chlorobium tepidum* (5). As a consequence, a single catalytic mechanism is likely to operate in SoxAX enzymes. Kappler *et al.* (36) have proposed an essential role for Cu(II) in SoxAX catalysis. The work presented here corroborates previous studies in finding no indication of a site for binding Cu(II) within the structure of the enzyme resolved by x-ray crystallography (36). Thus, we propose that the activity of SoxAX originates from its heme cofactors and/or their ligands.

The mechanism of SoxAX must account for the oxidative coupling of thiosulfate to the Cys^- of SoxY accompanied by the reduction of two molecules of cyt *c*. Bamford *et al.* (8) proposed a mechanism in which the thiolate ligand of Heme-2 dissociates to form a disulfide bond with thiosulfate in a process accompanied by the reduction of Heme-2 and -3 (Fig. 5*A*). In this mechanism, the oxidized thiosulfate is subsequently fused to the Cys^- of SoxY in a sulfur transferase step and the SoxAX is returned to the all-ferric state by the reduction of 2 equivalents of cyt *c*. The reactivity of dithionite treated SoxAX toward cyanide reported here provides the first evidence that the dissociation of $CysS^-$ from Heme-2, as required for this mechanism, can indeed occur.

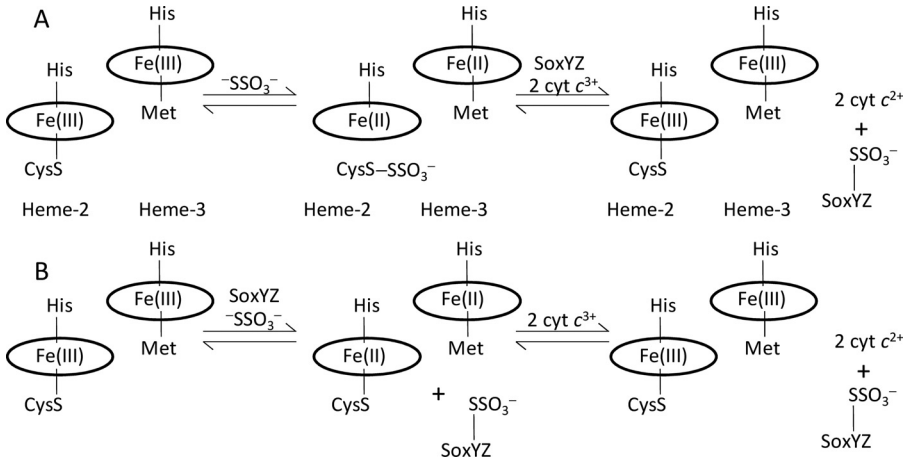

FIGURE 5. **Proposed mechanisms of SoxAX activity.** Reaction schemes for the SoxAX catalyzed attachment of thiosulfate to SoxYZ are shown. *Scheme A*, Cys-222A dissociates from Heme-2 and forms a disulfide bond with thiosulfate, liberating two electrons that reduce Heme-2 and -3 to the ferrous state. Subsequently, thiosulfate is transferred to SoxYZ, and SoxAX is returned to the resting state by the reduction of 2 equivalents of cyt *c*. *Scheme B*, thiosulfate binds directly to SoxYZ, liberating two electrons that reduce Heme-2 and -3 of SoxAX. Subsequent steps are as above. Cys-222A remains ligated to Heme-2 throughout.

Eu(II) reduces the SoxAX hemes as effectively as dithionite, but it does not act as a precursor for the displacement of the $CysS^-$ ligand to Heme-2 by cyanide. The dissociation of $CysS^-$ may then arise from the ability of dithionite and/or its oxidation products to mimic chemistry that can be induced by thiosulfate, the substrate of SoxAX. The details of this chemistry are unclear at present. The EPR of SoxAX following reduction with dithionite and equilibration with air demonstrates that Heme-2 retains a thiolate (RS^-, where R is any alkyl chain) ligand in the absence of CN^-. This is consistent with the reported structure of dithionite-reduced SoxAX where the $CysS^-$ ligand remains in place (8). However, it should be noted that the spectroscopic response of hemes with His/RS^- ligation is insensitive to the nature of R. It may be that Heme-2 is ligated by HS^- or Cys^- rather than $CysS^-$ in solutions of dithionite exposed SoxAX.

An alternative to the mechanism of Bamford *et al.* (8) can be proposed for SoxAX activity (Fig. 5*B*). In this mechanism, SoxAX mediates the direct coupling of thiosulfate to SoxY without dissociation of any heme ligands. To our knowledge, there are no reports for the E_m of the half-reaction relevant to the reduction of Heme-2 in this mechanism, namely, $CysSSO_3^- + 2e^- \leftrightarrow$ thiosulfate + Cys^-. A similar couple is that associated with Cys-Cys disulfide bonds and for which an $E_m < -250$ mV, or even < -400 mV for those serving a structural role, is not uncommon (37, 38). Thus, the couple formed by thiosulfate and the SoxY-Cys^- may be capable of reducing a minor proportion of the Heme-2 population. Forward reaction would then occur by electron transfer from Heme-2 to Heme-3, the higher E_m of the latter providing the thermodynamic driving force for product formation. The disparity in E_m between Heme-2 and both Heme-3 and the SoxYZ-thiosulfate couple would promote rapid electron transfer in either direction from reduced Heme-2. Therefore, any 1-electron oxidized species such as $SSO3^{\bullet -}$ or $Cys^{\bullet}$ formed by the initial reduction of Heme-2 would be short-lived, limiting the potential for damaging side reactions.

The high E_m of Heme-3 may also be relevant to controlling active site chemistry in the mechanism proposed by Bamford *et al.* (8) (Fig. 5*A*). However, the couple(s) relevant to describing this mechanism must include ferrous Heme-2 without $CysS^-$ ligation and most likely with His/water (hydroxide) ligation or in a pentacoordinate His-ligated state. For these ligand sets, the E_m is likely to be significantly greater than -400 mV because the low value in the enzyme as purified is thought to be a consequence of ligation by $CysS^-$. This makes it difficult to discount this mechanism, as has been proposed (36), on the basis of the E_m values reported for Heme-2. Indeed, given that $CysS^-$-ligated heme is so far unique to SoxAX enzymes, it seems most likely that this ligand and its dissociation from Heme-2, as demonstrated here, are key to thiosulfate oxidation.

Acknowledgments—We are grateful to Prof. James Durrant and Li Xiaoe (Imperial College London) for providing the SnO_2 electrodes used in this work and to Dr. Ulrike Kappler for providing plasmid pDOREX.

REFERENCES

1. Friedrich, C. G., Bardischewsky, F., Rother, D., Quentmeier, A., and Fischer, J. (2005) Prokaryotic sulfur oxidation. *Curr. Opin. Microbiol.* **8,** 253–259
2. Frigaard, N. U., and Dahl, C. (2009) in *Advances in Microbial Physiology*, Vol. 54 (Poole, R. K., ed) pp. 103–200, Elsevier Ltd., Oxford, UK
3. Sauvé, V., Bruno, S., Berks, B. C., and Hemmings, A. M. (2007) The SoxYZ complex carries sulfur cycle intermediates on a peptide swinging arm. *J. Biol. Chem.* **282,** 23194–23204
4. Quentmeier, A., and Friedrich, C. G. (2001) The cysteine residue of the SoxY protein as the active site of protein-bound sulfur oxidation of *Paracoccus pantotrophus* GB17. *FEBS Lett.* **503,** 168–172
5. Ogawa, T., Furusawa, T., Nomura, R., Seo, D., Hosoya-Matsuda, N., Sakurai, H., and Inoue, K. (2008) SoxAX binding protein, a novel component of the thiosulfate-oxidizing multienzyme system in the green sulfur bacterium *Chlorobium tepidum*. *J. Bacteriol.* **190,** 6097–6110
6. Dambe, T., Quentmeier, A., Rother, D., Friedrich, C., and Scheidig, A. J. (2005) Structure of the cytochrome complex SoxXA of *Paracoccus pantotrophus*, a heme enzyme initiating chemotrophic sulfur oxidation. *J. Struct. Biol.* **152,** 229–234
7. Cheesman, M. R., Little, P. J., and Berks, B. C. (2001) Novel heme ligation in a *c*-type cytochrome involved in thiosulfate oxidation: EPR and MCD of SoxAX from *Rhodovulum sulfidophilum*. *Biochemistry* **40,** 10562–10569
8. Bamford, V. A., Bruno, S., Rasmussen, T., Appia-Ayme, C., Cheesman, M. R., Berks, B. C., and Hemmings, A. M. (2002) Structural basis for the oxidation of thiosulfate by a sulfur cycle enzyme. *EMBO J.* **21,** 5599–5610
9. Kilmartin, J. R., Maher, M. J., Krusong, K., Noble, C. J., Hanson, G. R., Bernhardt, P. V., Riley, M. J., and Kappler, U. (2011) Insights into structure and function of the active site of SoxAX cytochromes. *J. Biol. Chem.* **286,** 24872–24881
10. Kappler, U., Aguey-Zinsou, K. F., Hanson, G. R., Bernhardt, P. V., and McEwan, A. G. (2004) Cytochrome c_{551} from *Starkeya novella*: characterization, spectroscopic properties, and phylogeny of a diheme protein of the SoxAX family. *J. Biol. Chem.* **279,** 6252–6260
11. Gliubich, F., Gazerro, M., Zanotti, G., Delbono, S., Bombieri, G., and Berni, R. (1996) Active site structural features for chemically modified forms of rhodanese. *J. Biol. Chem.* **271,** 21054–21061
12. Bordo, D., Forlani, F., Spallarossa, A., Colnaghi, R., Carpen, A., Bolognesi, M., and Pagani, S. (2001) A persulfurated cysteine promotes active site reactivity in *Azotobacter vinelandii* rhodanese. *Biol. Chem.* **382,** 1245–1252
13. Reijerse, E. J., Sommerhalter, M., Hellwig, P., Quentmeier, A., Rother, D., Laurich, C., Bothe, E., Lubitz, W., and Friedrich, C. G. (2007) The unusual redox centers of SoxXA, a novel *c*-type heme-enzyme essential for chemotrophic sulfur-oxidation of *Paracoccus pantotrophus*. *Biochemistry* **46,** 7804–7810
14. Male, L., Marritt, S. J., Berks, B. C., Cheesman, M. R., van Wonderen, J. H., George, S. J., and Butt, J. N. (2008) Protein voltammetry and spectroscopy: integrating approaches. *Theor. Chem. Account* **119,** 107–111
15. Du, J., Sono, M., and Dawson, J. H. (2011) The H93G myoglobin cavity mutant as a versatile scaffold for modeling heme iron coordination structures in protein active sites and their characterization with magnetic circular dichroism spectroscopy. *Coord. Chem. Rev.* **255,** 700–716
16. Gadsby, P. M., and Thomson, A. J. (1990) Assignment of the axial ligands of ferric iron in low-spin hemoproteins by near infrared magnetic circular dichroism and electron paramagnetic resonance spectroscopy. *J. Am. Chem. Soc.* **112,** 5003–5011
17. Kappler, U., and McEwan, A. G. (2002) A system for the heterologous expression of complex redox proteins in *Rhodobacter capsulatus*: characterisation of recombinant sulphite: cytochrome *c* oxidoreductase from. *Starkeya novella*. *FEBS Lett.* **529,** 208–214
18. Keen, N. T., Tamaki, S., Kobayashi, D., and Trollinger, D. (1988) Improved broad-host-range plasmids for DNA cloning in Gram-negative bacteria. *Gene* **70,** 191–197
19. Shaw, A. L., Leimkuhler, S., Klipp, W., Hanson, G. R., and McEwan, A. G. (1999) Mutational analysis of the dimethylsulfoxide respiratory (*dor*) operon of *Rhodobacter capsulatus*. *Microbiology* **145,** 1409–1420

20. Simon, R., Priefer, U., and Puhler, A. (1983) A broad host range mobilization system for *in vivo* genetic engineering: transposon mutagenesis in gram-negative bacteria. *Nat. Biotechnol.* **1,** 784–791
21. Weaver, P. F., Wall, J. D., and Gest, H. (1975) Characterization of *Rhodopseudomonas capsulata*. *Arch. Microbiol.* **105,** 207–216
22. Appia-Ayme, C., Little, P. J., Matsumoto, Y., Leech, A. P., and Berks, B. C. (2001) Cytochrome complex essential for photosynthetic oxidation of both thiosulfate and sulfide in *Rhodovulum sulfidophilum*. *J. Bacteriol.* **183,** 6107–6118
23. Kemp, G. L., Marritt, S. J., Xiaoe, L., Durrant, J. R., Cheesman, M. R., and Butt, J. N. (2009) Opportunities for mesoporous nanocrystalline SnO_2 electrodes in kinetic and catalytic analyses of redox proteins. *Biochem. Soc. Trans.* **37,** 368–372
24. Marritt, S. J., Kemp, G. L., Xiaoe, L., Durrant, J. R., Cheesman, M. R., and Butt, J. N. (2008) Spectroelectrochemical characterization of a pentaheme cytochrome in solution and as electrocatalytically active films on nanocrystalline metal-oxide electrodes. *J. Am. Chem. Soc.* **130,** 8588–8589
25. Astuti, Y., Topoglidis, E., Briscoe, P. B., Fantuzzi, A., Gilardi, G., and Durrant, J. R. (2004) Proton-coupled electron transfer of flavodoxin immobilized on nanostructured tin dioxide electrodes: Thermodynamics versus kinetics control of protein redox function. *J. Am. Chem. Soc.* **126,** 8001–8009
26. Marritt, S. J., van Wonderen, J. H., Cheesman, M. R., and Butt, J. N. (2006) Magnetic circular dichroism of hemoproteins with *in situ* control of electrochemical potential: "MOTTLE". *Anal. Biochem.* **359,** 79–83
27. Anderson, L. J., Richardson, D. J., and Butt, J. N. (2001) Catalytic protein film voltammetry from a respiratory nitrate reductase provides evidence for complex electrochemical modulation of enzyme activity. *Biochemistry* **40,** 11294–11307
28. Vincent, K. A., Tilley, G. J., Quammie, N. C., Streeter, I., Burgess, B. K., Cheesman, M. R., and Armstrong, F. A. (2003) Instantaneous, stoichiometric generation of powerfully reducing states of protein active sites using Eu(II) and polyaminocarboxylate ligands. *Chem. Comm.* (*Camb.*) 2590–2591
29. Dhawan, I. K., Shelver, D., Thorsteinsson, M. V., Roberts, G. P., and Johnson, M. K. (1999) Probing the heme axial ligation in the CO-sensing CooA protein with magnetic circular dichroism spectroscopy. *Biochemistry* **38,** 12805–12813
30. McKnight, J., Cheesman, M. R., Thomson, A. J., Miles, J. S., and Munro, A. W. (1993) Identification of charge-transfer transitions in the optical-spectrum of low-spin ferric cytochrome P-450 *Bacillus megaterium*. *Eur. J. Biochem.* **213,** 683–687
31. Walker, F. A. (1999) Magnetic spectroscopic (EPR, ESEEM, Mossbauer, MCD, and NMR) studies of low-spin ferriheme centers and their corresponding heme proteins. *Coord. Chem. Rev.* **185–6,** 471–534
32. Cheesman, M. R., Greenwood, C., and Thomson, A. J. (1991) Magnetic circular dichroism of hemoproteins. *Adv. Inorg. Chem.* **36,** 201–255
33. Yoshioka, S., Takahashi, S., Hori, H., Ishimori, K., and Morishima, I. (2001) Proximal cysteine residue is essential for the enzymatic activities of cytochrome $P450_{cam}$. *Eur. J. Biochem.* **268,** 252–259
34. Sono, M., Perera, R., Jin, S., Makris, T. M., Sligar, S. G., Bryson, T. A., and Dawson, J. H. (2005) The influence of substrate on the spectral properties of oxyferrous wild-type and T252A cytochrome P450-CAM. *Arch. Biochem. Biophys.* **436,** 40–49
35. Perera, R., Sono, M., Sigman, J. A., Pfister, T. D., Lu, Y., and Dawson, J. H. (2003) Neutral thiol as a proximal ligand to ferrous heme iron: Implications for heme proteins that lose cysteine thiolate ligation on reduction. *Proc. Natl. Acad. Sci. U.S.A.* **100,** 3641–3646
36. Kappler, U., Bernhardt, P. V., Kilmartin, J., Riley, M. J., Teschner, J., McKenzie, K. J., and Hanson, G. R. (2008) SoxAX cytochromes, a new type of heme copper protein involved in bacterial energy generation from sulfur compounds. *J. Biol. Chem.* **283,** 22206–22214
37. Ostergaard, H., Henriksen, A., Hansen, F. G., and Winther, J. R. (2001) Shedding light on disulfide bond formation: engineering a redox switch in green fluorescent protein. *EMBO J.* **20,** 5853–5862
38. Mishra, P., Socolich, M., Wall, M. A., Graves, J., Wang, Z., and Ranganathan, R. (2007) Dynamic scaffolding in a G protein-coupled signaling system. *Cell* **131,** 80–92